On the shape of giant soap bubbles

Caroline Cohen[a,1], Baptiste Darbois Texier[a,1], Etienne Reyssat[b,2], Jacco H. Snoeijer[c,d,e], David Quéré[b], and Christophe Clanet[a]

[a]Laboratoire d'Hydrodynamique de l'X, UMR 7646 CNRS, École Polytechnique, 91128 Palaiseau Cedex, France; [b]Laboratoire de Physique et Mécanique des Milieux Hétérogènes (PMMH), UMR 7636 du CNRS, ESPCI Paris/Paris Sciences et Lettres (PSL) Research University/Sorbonne Universités/Université Paris Diderot, 75005 Paris, France; [c]Physics of Fluids Group, University of Twente, 7500 AE Enschede, The Netherlands; [d]MESA+ Institute for Nanotechnology, University of Twente, 7500 AE Enschede, The Netherlands; and [e]Department of Applied Physics, Eindhoven University of Technology, 5600 MB, Eindhoven, The Netherlands

Edited by David A. Weitz, Harvard University, Cambridge, MA, and approved January 19, 2017 (received for review October 14, 2016)

We study the effect of gravity on giant soap bubbles and show that it becomes dominant above the critical size $\ell = a^2/e_0$, where e_0 is the mean thickness of the soap film and $a = \sqrt{\gamma_b/\rho g}$ is the capillary length (γ_b stands for vapor–liquid surface tension, and ρ stands for the liquid density). We first show experimentally that large soap bubbles do not retain a spherical shape but flatten when increasing their size. A theoretical model is then developed to account for this effect, predicting the shape based on mechanical equilibrium. In stark contrast to liquid drops, we show that there is no mechanical limit of the height of giant bubble shapes. In practice, the physicochemical constraints imposed by surfactant molecules limit the access to this large asymptotic domain. However, by an exact analogy, it is shown how the giant bubble shapes can be realized by large inflatable structures.

soap bubbles | Marangoni stress | self-similarity

Soap films and soap bubbles have had a long scientific history since Robert Hooke (1) first called the attention of the Royal Society and of Newton to optical phenomena (2). They have been of assistance in the development of capillarity (3) and of minimal surface problems (4). Bubbles have also served as efficient sensors for detecting the magnetism of gases (5), as elegant 2D water channels (6), and as analog "computers" in solving torsion problems in elasticity (7, 8), compressible problems in gas dynamics (9), and even heat conduction problems (10). Finally, in the last decades, the role of soap films and bubbles in the development of surface science has been crucial (11–13), and the ongoing activity in foams (14, 15) and in the influence of menisci on the shapes of bubbles (16) are modern illustrations of their key role. The shape of a soap bubble is classically obtained by minimizing the surface energy for a given volume, hence resulting to a spherical shape. However, the weight of the liquid contained in the soap film is always neglected, and it is the purpose of this article to discuss this effect.

For liquid drops, the transition from a spherical cap drop to a puddle occurs when the gravitational energy, $\rho g R^4$ (R is the typical size of the drop), becomes of the same order as its surface energy $\gamma_b R^2$. That is, for a drop size of the order of the capillary length $a = \sqrt{\gamma_b/\rho g}$ (γ_b is the liquid–vapor surface tension, and ρ is the liquid density). Typically, this transition is observed at the millimetric scale: For a soap solution with $\gamma_b = 30$ mN/m, $a \simeq 1.7$ mm. The two asymptotic regimes may be distinguished through the behavior of the drop height h_0 with volume: $h_0 \approx R$ for small spherical drops, while the height of large puddles saturates to a constant value $h_0 \approx a$.

If we look for the same transition in soap bubbles, we expect the gravitational energy, $\rho g R^3 e_0$, to become of the order of the surface energy, $\gamma_b R^2$, at the typical size $R \approx \ell$, with $\ell = a^2/e_0$ (e_0 stands for the mean thickness of the film). Thanks to the iridescence, the mean thickness can be estimated to a few microns or less, and the light–heavy transition is thus expected at the metric scale (instead of the millimetric one for drops): For $\gamma_b = 30$ mN/m and $e_0 = 1\mu$m, $\ell \simeq 3.1$ m.

The experimental setup dedicated to the study of such large bubbles is presented in *Experimental Setup*, before information on *Experimental Results* and *Model*. The discussion on the asymptotic shape and the analogy with inflated structures is presented in *Analogy with Inflatable Structures*.

Experimental Setup

The soap solution is prepared by mixing two volumes of Dreft© dishwashing liquid, two volumes of water, and one volume of glycerol and was left aside for 10 h before experiments. The surface tension of the different mixtures was measured using the pendant drop method. It was found to be $\gamma_b = 26 \pm 1$ mN/m.

The bubbles are formed in a round inflated swimming pool of 4 m diameter (Fig. 1), filled with 10 cm to 20 cm of soap solution. A large bubble wand was assembled with two wood sticks and two cotton strings. The strings were immersed in the soap solution. Two experimenters, located on opposite sides of the pool, slowly opened the loop in air and pulled the sticks above the water surface, before dipping the loop into the water to form the bubble.

Once the bubble is at rest, the shape is analyzed by side view images as shown in Fig. 1. In particular, we measure the diameter, $2R$, and the height, h_0, of the giant bubble. The camera is placed 4 m from the center of the pool, and the center of the lens is at the same height as the center of the bubble, to minimize parallax errors.

The film thickness e_0 is important when studying the effect of the bubble weight, as it determines the liquid mass. Following McEntee and Mysels (17), the thickness of the bubble is measured via the bursting technique: A hole in a punctured soap film

Significance

Surface tension dictates the spherical cap shape of small sessile drops, whereas gravity flattens larger drops into millimeter-thick flat puddles. In contrast with drops, soap bubbles remain spherical at much larger sizes. However, we demonstrate experimentally and theoretically that meter-sized bubbles also flatten under their weight, and we compute their shapes. We find that mechanics does not impose a maximum height for large soap bubbles, but, in practice, the physicochemical properties of surfactants limit the access to this self-similar regime where the height grows as the radius to the power 2/3. An exact analogy shows that the shape of giant soap bubbles is nevertheless realized by large inflatable structures.

Author contributions: C. Cohen, B.D.T., and C. Clanet designed research; C. Cohen, B.D.T., E.R., J.H.S., and C. Clanet performed research; C. Cohen, B.D.T., E.R., J.H.S., D.Q., and C. Clanet analyzed data; and C. Cohen, B.D.T., E.R., J.H.S., and C. Clanet wrote the paper.

The authors declare no conflict of interest.

This article is a PNAS Direct Submission.

[1]C. Cohen and B.D.T. contributed equally to this work.

[2]To whom correspondence should be addressed. Email: etienne.reyssat@espci.fr.

This article contains supporting information online at www.pnas.org/lookup/suppl/doi:10.1073/pnas.1616904114/-/DCSupplemental.

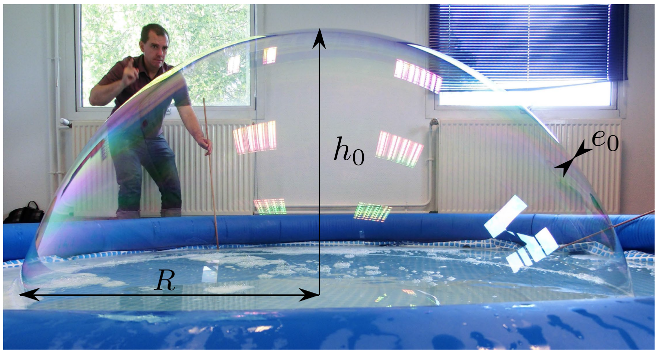

Fig. 1. Presentation of a "giant" soap bubble and definition of its radius, R, and height, h_0. (Here, $R = 1.09$ m, and $h_0 = 0.97$ m.)

grows because of unbalanced surface tension forces at the edge of the hole. The opening velocity v is constant and is given by the Dupré–Taylor–Culick law (18–20),

$$v^2 = \frac{2\gamma_b}{\rho e_0} = 2g\ell, \qquad [1]$$

where $\gamma_b \simeq 26$ mN/m, and $\rho \simeq 1{,}000\ \mathrm{kg{\cdot}m^{-3}}$. Examples of thickness measurements are presented in Fig. 2: In Fig. 2*A* and Fig. 2*B*, we present two sequences of four pictures showing the opening of a hole in two soap bubbles of different sizes. We use such sequences to extract the bursting velocity plotted as a function of time in Fig. 2*C*. We observe that v is almost constant and takes the value of 8 m/s for sequence in Fig. 2*A* and 2.8 m/s for sequence in Fig. 2*B*. From the value of v, we deduce $e_0 \simeq 0.81\ \mu$m and $\ell \approx 3.2$ m for Fig. 2*A* and $e_0 \simeq 6.6\ \mu$m and $\ell \approx 0.4$ m for Fig. 2*B*, using Eq. **1**. Although it may seem surprising to find that the film thickness is homogeneous, earlier studies on the drainage of almost spherical liquid shells have shown that the thickness approaches a profile with little spatial variations (21, 22).

Experimental Results

Once ℓ is determined, we use it to rescale the experimental shapes. An example of a nonspherical bubble is presented in reduced scale in Fig. 3*A*. A systematic analysis of the effect of gravity on the bubble shape is shown in Fig. 3*B*, where we plot the reduced height h_0/ℓ as a function of the bubble reduced radius R/ℓ for all experiments. Fig. 3*B* reveals that the bubbles' shapes remain approximately spherical ($h_0/\ell = R/\ell$, black dashed line) only up to $R/\ell \approx 0.3$. For larger sizes, the bubble height is significantly lower than that of a sphere. The largest value of h_0/ℓ reached experimentally is ~ 1.2, with corresponding radius $R/\ell = 1.6$. Two points must be underlined at this stage: (*i*) The experimental data in Fig. 3*B* show no sign of a height saturation for increased bubble volumes, and (*ii*) despite our efforts, we never managed to make bubbles larger than $R = 1$ m. Both observations will be explained in *Model*.

Model

We now consider the mechanical equilibrium of the soap film and predict how gravity affects the bubble shape. Bubbles are axisymmetric, and we assume a uniform film thickness e_0. The bubble shape is described using the parametrization shown in Fig. 4 *A* and *B*: The local height of the soap film is $h(s)$, and the local angle of the membrane relative to the horizontal is $\theta(s)$ (defined as positive everywhere). The height and angle are functions of the curvilinear coordinate s that measures the arclength starting from the top of the bubble; φ is the azimuthal angle around the vertical axis.

The equilibrium of an infinitesimal part of the membrane of surface area $r\mathrm{d}s\mathrm{d}\varphi$ is first considered along the s direction. To account for the experimentally observed slow draining and long bubble lifetimes, the air–liquid interface must strongly moderate the flow and behave as partially rigid, in contrast with the no-stress behavior of surfactant-free interfaces. The main effect is that gradients in surface tension $\gamma(s)$, due to the presence of surfactants, have to balance viscous stresses applied by the flowing liquid along the interface. In reaction, viscous stresses balance the weight of the liquid in the film. Finally, the weight of liquid is fully transmitted to the walls through viscous stresses and balanced by surface tension gradients (15). The contribution due to surface tension on each side of the infinitesimal element gives a force $2\gamma r\mathrm{d}\varphi$, where γ is a function of position s. The weight of the liquid inside the film is $\rho g e_0 r\mathrm{d}\varphi\mathrm{d}s\,\sin\theta$, when projected along the s direction. The balance of surface tension and weight thus gives

$$2r\mathrm{d}\varphi\,[\gamma(s) - \gamma(s+\mathrm{d}s)] = \rho g e_0 r\mathrm{d}\varphi\mathrm{d}s\,\sin\theta, \qquad [2]$$

which, using $\mathrm{d}h/\mathrm{d}s = -\sin\theta$, yields

$$\mathrm{d}\gamma = \frac{1}{2}\rho g e_0 \mathrm{d}h \quad \Rightarrow \quad \gamma(s) = \gamma_b + \frac{1}{2}\rho g e_0 h(s). \qquad [3]$$

Here γ_b is the surface tension of the soap solution at the base of the bubble ($h = 0$), and the surface tension is found to increase

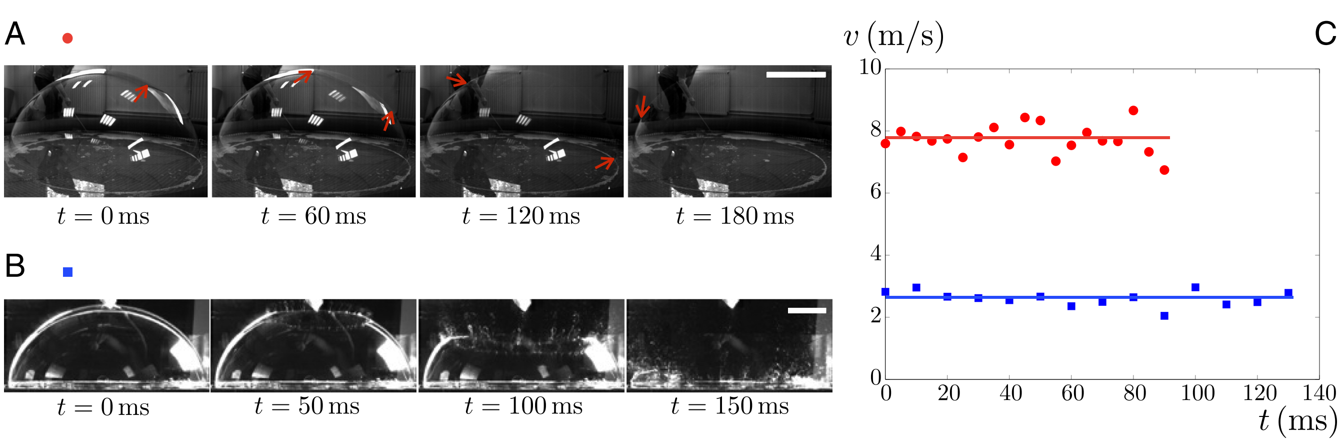

Fig. 2. Bursting of bubbles used to determine the soap film thickness. (*A*) Image sequence of bursting bubbles, with a time step of 60 ms between images. Red arrows indicate the boundary of the opening hole on each image. (Scale bar, 50 cm.) (*B*) Bursting sequence with a time step of 50 ms between images. (Scale bar, 10 cm.) (*C*) The bursting velocity corresponding to *A* and *B* is plotted versus time.

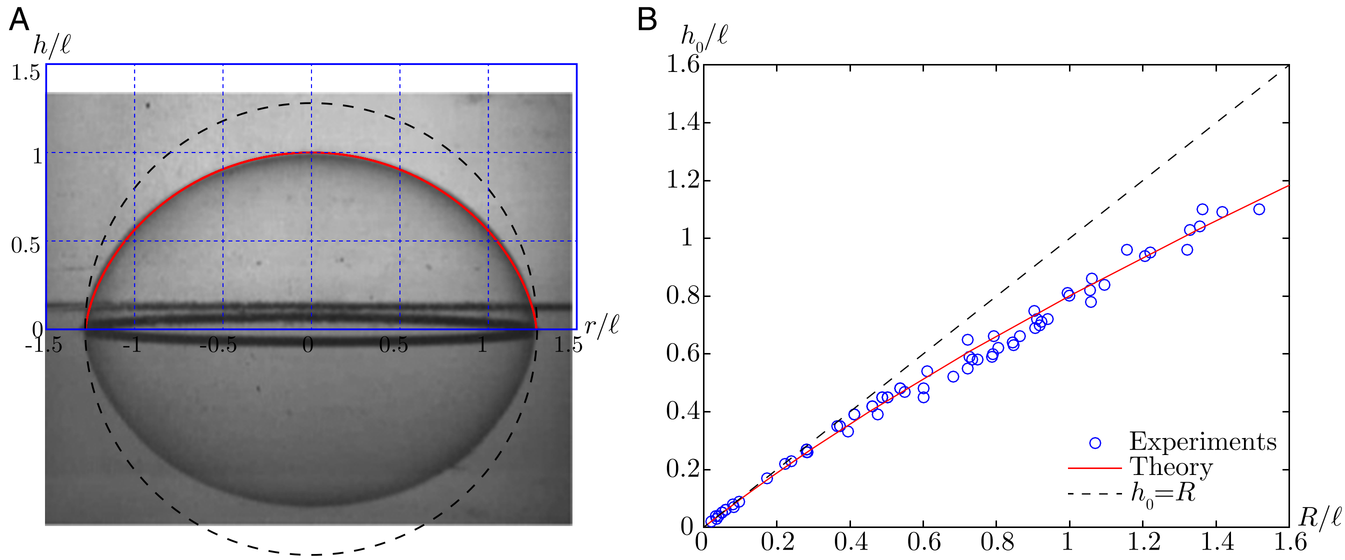

Fig. 3. (*A*) Example of flattened soap bubble of equatorial diameter 20 cm. The black dashed line is a circle, and the red solid line is the theoretical shape obtained through the numerical integration of Eq. **6** that gives the same aspect ratio h_0/R as the experiment. (*B*) Flattening of soap bubbles due to gravity, quantified by the scaled height h_0/ℓ as a function of the scaled radius R/ℓ, where $\ell = a^2/e_0$. Circles represent experimental data, the solid red line stands for the model prediction, and the dashed black line represents the spherical limit $h_0 = R$.

with height (23). For a bubble of thickness $e_0 = 1\,\mu$m and height 1 m, the surface tension contrast between the base and top of the bubble is typically 5 mN/m.

A closed equation for the bubble shape is obtained when next considering the equilibrium normal to the membrane. The pressure difference ΔP between the inside and outside of the bubble, to balance the weight projected normal to the film $\rho g e_0 \cos\theta$ and the Laplace pressure due to the two curved liquid–air interfaces. The balance of pressure and weight reads

$$\Delta P = 2\gamma(s)\left(\frac{\mathrm{d}\theta}{\mathrm{d}s} + \frac{\sin\theta}{r}\right) + \rho g e_0 \cos\theta, \qquad [4]$$

where $\mathrm{d}\theta/\mathrm{d}s$ is the curvature along s and $\sin\theta/r$ is other principal curvature for an axisymmetric surface. We remind that $\gamma(s)$ is given by Eq. **3**. As a final step, it is convenient to eliminate ΔP by its value at the top of the bubble ($s = 0$, $\theta = 0$, and $h = h_0$), where $(\mathrm{d}\theta/\mathrm{d}s + \sin\theta/r)|_{s\to 0} \to 2\mathrm{d}\theta/\mathrm{d}s|_{s=0}$ and $\gamma(s=0) = \gamma_b + 1/2\rho g e_0 h_0$. Combining $\Delta P\,(s=0)$ with Eqs. **3** and **4** gives the equation for the shape of the bubble,

$$(2\gamma_b + \rho g e_0 h)\left(\frac{\mathrm{d}\theta}{\mathrm{d}s} + \frac{\sin\theta}{r} - 2\left.\frac{\mathrm{d}\theta}{\mathrm{d}s}\right|_{s=0}\right) - \rho g e_0\left(1 - \cos\theta + 2(h_0 - h)\left.\frac{\mathrm{d}\theta}{\mathrm{d}s}\right|_{s=0}\right) = 0. \qquad [5]$$

Scaling all lengths with $\ell = a^2/e_0$, denoting scaled variables by a tilde, we obtain the shape equation in dimensionless form,

$$\left(2 + \tilde{h}\right)\left(\frac{\mathrm{d}\theta}{\mathrm{d}\tilde{s}} + \frac{\sin\theta}{\tilde{r}} - 2\left.\frac{\mathrm{d}\theta}{\mathrm{d}\tilde{s}}\right|_{\tilde{s}=0}\right) - \left(1 - \cos\theta + 2(\tilde{h}_0 - \tilde{h})\left.\frac{\mathrm{d}\theta}{\mathrm{d}\tilde{s}}\right|_{\tilde{s}=0}\right) = 0. \qquad [6]$$

A unique bubble shape is found numerically for each value of the dimensionless height $\tilde{h}_0$; this is done by adjusting the value of $\mathrm{d}\theta/\mathrm{d}\tilde{s}(\tilde{s} = 0)$ by a shooting algorithm to match the boundary conditions ($\tilde{h} = \tilde{h}_0$ and $\theta = 0$ at the top, with $\theta = \pi/2$ at $\tilde{h} = 0$ at the bath).

Fig. 4*C* shows the corresponding bubble shapes for increasing volume. As expected, small bubbles are dominated by surface tension and are perfectly spherical. However, as bubbles get larger ($\tilde{h}_0 > 1$), they show a tendency to flatten with respect to the spherical shape. A direct comparison of the theoretical shape with a real bubble is presented in Fig. 3*A*, where we superimpose the picture of a 20-cm diameter bubble with the solution of Eq. **6** that has the same ratio h_0/R. The two shapes cannot be distinguished. The model (Eq. **6**) also gives a quantitative prediction for the height $\tilde{h}_0 = h_0/\ell$ versus $\tilde{R} = R/\ell$ that can be compared with the experimental data in Fig. 3*B* (solid line). The result describes very well, without any adjustable parameter, the experimentally observed flattening due to gravity.

Unexpectedly, the numerical solution does not predict a saturation of the bubble height: $\tilde{h}_0$ continues to increase in the limit of large volume. This feature is highlighted in more detail in Fig. 4*E*, showing the dimensionless bubble height on a log–log plot. For large volumes, we find that $\tilde{h}_0 \approx \tilde{R}^{2/3}$. This scaling law implies a decaying aspect ratio, i.e., $\tilde{h}/\tilde{R} \ll 1$, but, at the same time, there is no saturation of the bubble height. Interestingly, these asymptotic features cannot be derived on simple dimensional grounds. According to Eq. **3**, both surface tension and gravity scale with $\rho g e_0$, which points to a scale invariance at large bubble heights. Indeed, as is shown in *Supporting Information*, the large bubble shapes in Fig. 4*C* exhibit scale invariance and can be collapsed to a single, universal shape. The scaling of the universal shape near the edge reads $\tilde{h} \approx (\tilde{R} - \tilde{r})^{2/3}$, as can be inferred from the dominant balance $\tilde{h}\mathrm{d}\theta/\mathrm{d}s = (\cos\theta - 1) \simeq h'^2/2$ in Eq. **6**. The 2/3 scaling at the edge determines the horizontal and vertical scales for the bubble and leads to the scaling in Fig. 4*E* (see *Supporting Information* for detailed analysis).

This scaling law for large bubbles, and, in particular, the lack of saturation, is in stark contrast with the classical result for liquid drops. The shape of droplets can be found from the classical hydrostatic pressure balance (13) and is different from Eq. **6**,

$$2\left(\frac{\mathrm{d}\theta}{\mathrm{d}\hat{s}} + \frac{\sin\theta}{\hat{r}} - 2\left.\frac{\mathrm{d}\theta}{\mathrm{d}\hat{s}}\right|_{\hat{s}=0}\right) - (\hat{h}_0 - \hat{h}) = 0. \qquad [7]$$

Here, the lengths were made dimensionless using the capillarity length $a = \sqrt{\gamma_b/\rho g}$, and denoted by hatted variables.

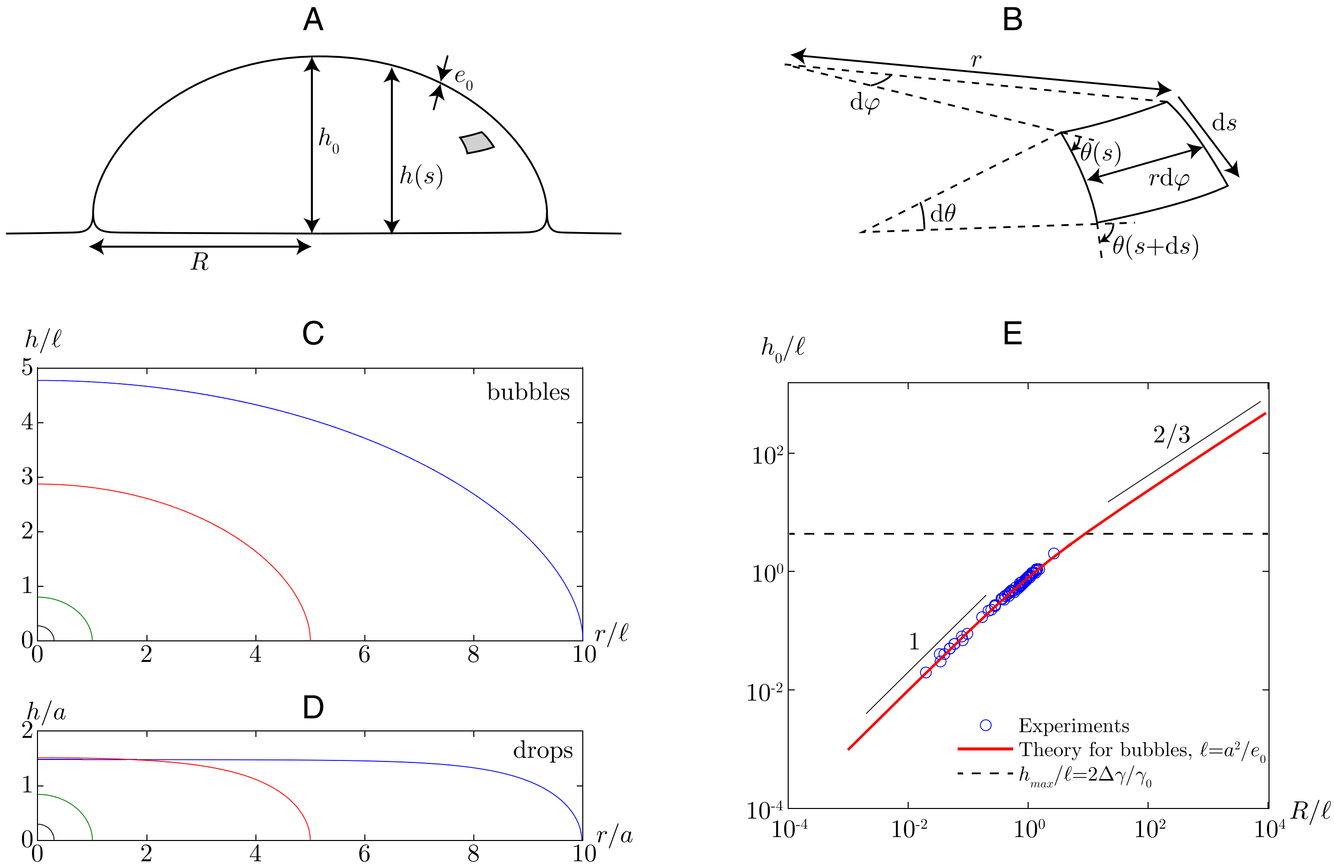

Fig. 4. (*A*) Sketch of a giant bubble of radius R and height h_0. The local height is h. The gray area shows an infinitesimal surface element of the bubble. (*B*) Zoom on the infinitesimal part of the bubble located at distance r from the symmetry axis of the bubble. The surface area of this surface element is $r\mathrm{d}s\mathrm{d}\varphi$; $\tan\theta$ is the local slope of the soap film with respect to the horizontal. (*C*) Shapes of soap bubbles with dimensionless radius $R/\ell = 0.3$, 1, 5, and 10. Although large bubbles tend to flatten (i.e., $h_0/R \to 0$), the height of giant bubbles shows no sign of saturation. (*D*) Shapes of liquid drops with contact angle $\theta = 90^\circ$ and dimensionless radius $R/a = 0.3$, 1, 5, and 10. The dimensionless height of large drops saturate to $\sqrt{2}$. (*E*) Experimental dimensionless height of soap bubbles as a function of their dimensionless radius (circles). The theoretical dimensionless height h_0/ℓ of bubbles (full line) is plotted as a function of their dimensionless radius R/ℓ. Small bubbles ($R/\ell < 0.3$) are insensitive to gravity and remain hemispherical, thus minimizing their surface area for the given volume. Giant bubbles flatten, but there is no saturation height as exists for drops larger than the capillary length: For large bubbles, one finds $h_0 \approx R^{2/3}$. The physical chemistry of surfactants, however, limits the range of accessible surface tension, setting the actual upper limit for the size of giant bubbles (dashed line): $h_{max}/\ell = 2\Delta\gamma/\gamma_b$.

Fig. 4*D* shows the corresponding numerical solutions: Large drops develop toward puddles, which, for $\theta = \pi/2$, saturate to the height $\hat{h}_0 = \sqrt{2}$.

The height of soap bubbles may, however, be limited by physical chemistry of surfactants. The water that constitutes the bubble is prevented from draining quickly by gradients in the surface tension. The larger surface tension at the top of the bubble supports the weight of water in the liquid shell (15). In practice, the surface tension of a soap solution cannot be higher than that of pure water, γ^*; γ also has a minimum, γ_b, set by the surfactant concentration of the solution used in the experiments. Eq. **3** thus gives a criterion for the maximal height h_{max} of the bubble,

$$\gamma^* = \gamma_b + \frac{1}{2}\rho g e_0 h_{max} \qquad \textbf{[8]}$$

so that

$$\frac{h_{max}}{\ell} = \frac{2\Delta\gamma}{\gamma_b}, \qquad \textbf{[9]}$$

where $\Delta\gamma = \gamma^* - \gamma_b$ is the highest achievable surface tension contrast between the top and bottom of a bubble; $\gamma^* \simeq 70$ mN/m, and γ_b may typically be as low as 20 mN/m, so that the expected maximal height of a bubble of thickness $e_0 = 5$ μm is of order 2 m, close to the size of the biggest bubbles we experimentally produced (Fig. 1).

Fig. 5. Festo's Airquarium, 31 m in diameter.

Analogy with Inflatable Structures

Interestingly, the shapes we have just discussed correspond to a minimization problem that is relevant in the context of large inflatable structures, such as shown in Fig. 5. These structures consist of a thin sheet that we assume cannot be stretched, and which is inflated by a pressure difference ΔP. The mechanical analysis on an infinitesimal element of the thin sheet is strictly equivalent to that in Fig. 4 *A* and *B*: The role of surface tension is replaced by the tension that develops inside the membrane. It is interesting to confirm this analogy based on energy minimization, with the no-stretch condition imposed through a Lagrange multiplier λ. Characterizing the axisymmetric shape as $h(r)$, and thus $h' = dh/dr$, the functional $\mathcal{F}[h]$ to be minimized reads

$$\mathcal{F}[h] = \int dr 2\pi r \mathcal{L}(h, h'), \qquad \textbf{[10]}$$

with

$$\mathcal{L}(h, h') = \rho g e_0 h (1 + h'^2)^{1/2} + \lambda (1 + h'^2)^{1/2} - \Delta P\, h. \qquad \textbf{[11]}$$

The three terms respectively represent the gravitational free energy, the area constraint, and the work done by the pressure difference. The Euler–Lagrange equation for this functional gives (see *Inflatable Structures*):

$$\Delta P = (\lambda + \rho g e_0 h) \left(\frac{\mathrm{d}\theta}{\mathrm{d}s} + \frac{\sin\theta}{r} \right) + \rho g e_0 \cos\theta, \qquad \textbf{[12]}$$

which is, indeed, strictly identical to the equation that dictates the bubble shapes (Eq. **4**). Designing the inflatable structures along these optimal shapes will naturally avoid stretching and compression of various parts of the sheets, avoiding wrinkles and reducing tensile stresses exerted in the sheets and on the seams that connect the various parts. This design should help increase the lifetime of such structures.

Conclusion

We study the shape of large soap bubbles and show that gravity becomes important at the scale $\ell = a^2/e_0$. We derive the equation for the shape and show that gravity matters in two distinct terms: the expected hydrostatic term and the evolution of surface tension via Marangoni stresses. A direct consequence is that there is a physicochemical limit to the size of soap bubbles, h_{max}. Finally, we point out that, contrary to drops, the shape of giant soap bubbles is not characterized by a saturation of the height but by a self-similar behavior in which $h_0/\ell \approx (R/\ell)^{2/3}$.

ACKNOWLEDGMENTS. We thank Tomas Bohr for organizing the 2013 Krogerup Summer School that initiated the collaboration between Paris and Twente. We also thank Isabelle Cantat for her input on the stability of soap films and for her constructive criticism of the initial version of our work.

1. Hooke R (1672) On holes (black film) in soap bubbles. *Commun R Soc* Mar 28.
2. Newton SI (1730) *Opticks or, A Treatise of the Reflections, Refractions, Inflections, and Colours of Light* (R Soc, London).
3. Plateau J (1873) *Statique Expérimentale Et Théorique Des Liquides Soumis Aux Seules Forces Moléculaires* (Gauthier-Villars, Paris).
4. Courant R, Robbins H (1941) *What Is Mathematics?* (Oxford Univ Press, London).
5. Faraday M (1851) Experimental researches in electricity. *Philos Trans R Soc London* 141:7–28.
6. Couder Y, Chomaz JM, Rabaud M (1989) On the hydrodynamics of soap films. *Physica D* 37:384–405.
7. Prandtl L (1903) Zur torsion von prismatischen stäben. *Phys Z* 4:758–770.
8. Griffith AA, Taylor GI (1917) The use of soap films in solving torsion problems. *Advis Comm Aeronaut Tech Rep* 333(3):920–937.
9. Wen CY, Lai JY (2003) Analogy between soap film and gas dynamics. I. Equations and shock jump conditions. *Exp Fluids* 34:107–114.
10. Wilson LH, Miles AJ (1950) Application of the membrane analogy to the solution of heat conduction problems. *J Appl Phys* 21:532–535.
11. Mysels KJ, Shinoda K, Frankel S (1959) *Soap Films: Studies of Their Thinning* (Pergamon, Oxford).
12. Isenberg C (1992) *The Science of Soap Films and Soap Bubbles* (Dover, Mineola, NY).
13. de Gennes PG, Brochard-Wyart F, Quéré D (2004) *Capillarity and Wetting Phenomena* (Springer, New York).
14. Petit P, Seiwert J, Cantat I, Biance A (2015) On the generation of a foam film during a topological rearrangement. *J Fluid Mech* 763:286–301.
15. Saulnier L, et al. (2014) A study of generation and rupture of soap films. *Soft Matter* 10:2899–2906.
16. Teixeira MA, Arscott S, Cox SJ, Teixeira PI (2015) What is the shape of an air bubble on a liquid surface? *Langmuir* 31:13708–13717.
17. McEntee WR, Mysels KJ (1969) The bursting of soap films. I. An experimental study. *J Phys Chem* 73(9):3018–3028.
18. Dupré A (1867) *Annales de Chimie et de Physique* 11(4):194.
19. Taylor GI (1959) The dynamics of thin sheets of fluid III. Disintegration of fluid sheets. *Proc R Soc A* 253:313–321.
20. Culick F (1960) Comments on a ruptured soap film. *J Appl Phys* 31:1128–1129.
21. Couder Y, Fort E, Gauthier CH, Boudaoud A (2005) From bouncing to floating: Non-coalescence of drops on a fluid bath. *Phys Rev Lett* 94:177801.
22. Lee A, et al. (2016) Fabrication of slender elastic shells by the coating of curved surfaces. *Nat Commun* 7:11155.
23. de Gennes PG (2001) "Young" soap films. *Langmuir* 17:2416–2419.